Inductive Power Transfer Efficiency Limit of a Flat Half-Filled Disc Coil Pair

Michael Leibl, Oliver Knecht, and Johann W. Kolar, *Fellow, IEEE*

***Abstract*—The efficiency limit for an inductive power transfer between two flat half-filled disc coils is derived based on a model for the eddy current losses in the coils and the losses due to electromagnetic radiation. Analytic approximations for the coupling factor of the coils and eddy current losses are proposed and experimentally verified. It is shown that the approximative terms allow us to express the maximum efficiency of the coil pair analytically. If the strand diameter of the coil is sufficiently small, the efficiency depends only on the strand diameter, diameter of the coils, and the gap between the coils—but not on the operating frequency. Therefore, increasing the frequency does not result in higher efficiency but allows to reduce the coil thickness.**

***Index Terms*—Eddy currents, inductive power transmission, Q-factor.**

Nomenclature

$\approx$	Approximately equal.
δ	Skin depth.
η_{12}	Primary coil to secondary coil efficiency.
γ	Effective magnetic field length per coil width.
$\hat{I}_{\mathrm{r}}$	Current amplitude per strand.
ω	Coil current angular frequency.
σ	Electrical conductivity.
$\simeq$	Asymptotically equal.
φ	Coil current phase angle.
c_0	Speed of light in vacuum.
d	Coil diameter.
F_{r}	Skin effect function for round wire.
g	Gap between coils.
G_{r}	Proximity effect function for round wire.
h	Coil height.
H_{srms}	Spatial RMS value of magnetic field.
I	Coil RMS current.
k	Coupling coefficient.
k_{cu}	Winding filling factor.
L	Coil inductance.
l_{h}	Effective magnetic field length.
M	Magnetic dipole moment.
N	Coil number of turns.
P_{ohm}	Coil ohmic loss.
P_{rad}	Coil dipole radiation loss.
P'_{r}	Dissipated power per unit length per strand.
P_{12}	Power transfer from primary to secondary coil.
Q	Coil quality factor.
R	Coil resistance.
R_{dc}	Coil dc resistance.
R_{ohm}	Coil ohmic resistance.
$R'_{\mathrm{r,dc}}$	Strand dc resistance per unit length.
R_{rad}	Coil dipole radiation resistance.
w	Coil width.

Manuscript received October 5, 2017; revised December 3, 2017; accepted January 11, 2018. Date of publication January 24, 2018; date of current version August 7, 2018. Recommended for publication by Associate Editor C. T. Rim. *(Corresponding author: Michael Leibl.)*

The authors are with the Department of Information Technology and Electrical Engineering, Power Electronic Systems Laboratory, ETH Zurich, Zurich Zurich Switzerland (e-mail: michael.leibl@icloud.com; knecht@lem.ee.ethz.ch; kolar@lem.ee.ethz.ch).

Color versions of one or more of the figures in this paper are available online at http://ieeexplore.ieee.org.

Digital Object Identifier 10.1109/TPEL.2018.2797366

I. Introduction

THE losses of an unshielded pair of inductive power transfer (IPT) coils can be divided into two groups. First, there are the ohmic losses of the current flowing in the coils and the eddy currents induced by the magnetic field. Second, the coil pair represents a magnetic dipole, which is radiating energy in the form of electromagnetic waves. Together these loss mechanisms limit the efficiency of an IPT system. Previous work in the field provides an expression for the coil pair efficiency limit [1]–[3], relying on two key parameters, i.e., quality factor and coupling coefficient which have to be determined numerically by a finite element method (FEM) simulation.

This work derives analytic expressions to calculate the maximum coil pair efficiency for flat half-filled disc coils. The intention is to provide the reader with an easy-to-use model in order to evaluate if the IPT could be a possible solution for a problem at hand and if very high operating frequencies [4], [5] could increase the coil pair efficiency. The presented approach cannot eliminate a numeric multiobjective optimization [6], [7] at a final stage of the design process, since the expressions cover only the case of a pair of magnetically unshielded (no core losses) flat half-filled coaxially aligned disc coils. However, the simple structure of the analytic expressions provides valuable insight on the way different geometric parameters affect the coil pair efficiency.

In Section II, the expression for the power transfer between two coupled coils is provided and applied to the case of a pair of half-filled disc coils. Models for ohmic (including eddy current) and radiation losses are derived and experimentally verified in Section III, which finally lead to the efficiency limit presented in Section IV. The result is discussed and conclusions are drawn in Section V.

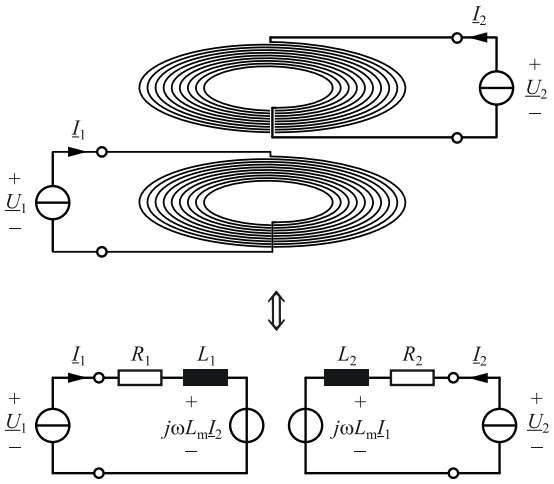

Fig. 1. Two coupled coils and their equivalent circuit.

II. Inductive Power Transfer

Assuming a pair of two coils as shown in Fig. 1, each coil can be represented by an equivalent circuit comprising a resistance, an inductance, and a voltage source equaling the voltage induced by the other coil. The induced voltage in one coil is proportional to the time derivative of the current in the other coil. The proportionality factor is called the mutual inductance L_m. For sinusoidal quantities, the time derivative is represented by $j\omega$, resulting in the induced voltages[1] shown in the equivalent circuit of Fig. 1. The active power transferred from the primary coil (index 1) to the secondary coil (index 2) equals the active power consumed by the equivalent voltage source $j\omega L_\mathrm{m}\underline{I}_2$ on the primary side, which can be expressed as

$$P_{12} = \Re\{j\omega L_\mathrm{m}\underline{I}_2\underline{I}_1^*\} = \omega L_\mathrm{m} I_1 I_2 \sin(\varphi_1 - \varphi_2). \quad (1)$$

The mutual inductance can be determined from

$$L_\mathrm{m} = k\sqrt{L_1 L_2} \quad (2)$$

with the self-inductances L_1, L_2 and the coupling coefficient k of the coil pair. For the case of an infinitely flat ($h \to 0$), half-filled (inner diameter equals half the outer diameter) disc coil as shown in Fig. 2, the self-inductance is obtained from an FEM simulation as

$$L \approx 0.76\mu_0 d N^2. \quad (3)$$

The coupling coefficient for the situation in Fig. 2 is also calculated using an FEM simulation and can be approximated with less than 3% error by the empirically found curve fit

$$k \approx \frac{1}{\left(1 + 3.2\left(\frac{g}{d}\right)^2\right)\left(1 + 7\frac{g}{d}\right)}. \quad (4)$$

The comparison of the curve fit and a measurement of the coupling coefficient with the FEM simulation is shown in Fig. 3, indicating very good agreement of measurement and fit. The measurement has been obtained on a coil pair with $d = 10$ cm, $h = 0.8$ mm, and $N_1 = N_2 = 31$ using 60×71 µm litz wire. The measured self-inductance of a coil is 89 µH, which agrees well with the calculated value of 92 µH according to (3).

Due to the good accuracy, the given approximations for self- and mutual inductance are used throughout the rest of this work. Except for FEM simulations, only a relatively complex semianalytic approach [8] is available to calculate the exact values.

[1]Upper-case letters indicate the RMS values. Complex phasor quantities are marked with underline, e.g., the phasor $\underline{I}_1 = I_1 e^{j\varphi_1}$ represents the current $i_1(t) = \sqrt{2} I_1 \cos(\omega t + \varphi_1)$.

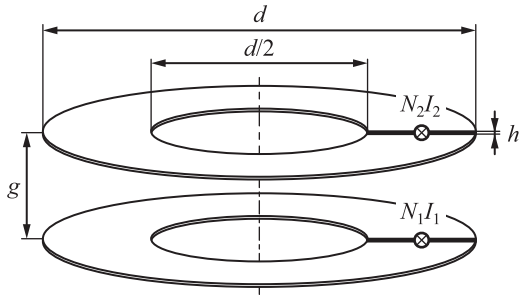

Fig. 2. Pair of two magnetically coupled flat coaxial half-filled disc coils with dimensions. The total amp turns NI of each coil are assumed to be homogeneously distributed over the coil cross-section.

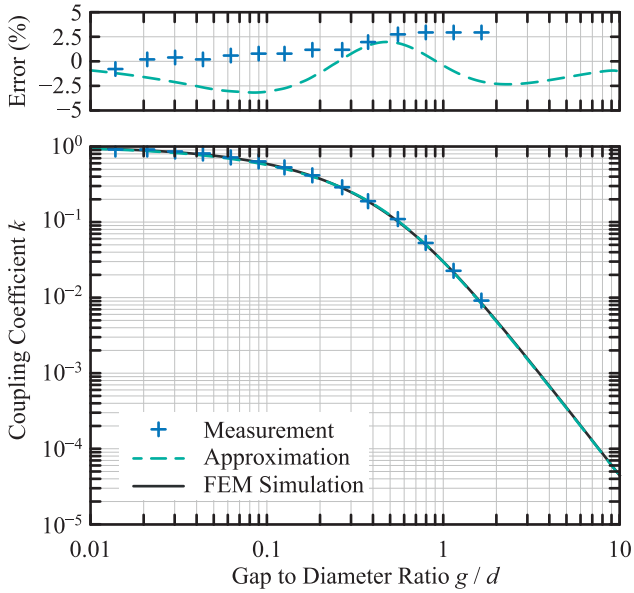

Fig. 3. Coupling coefficient of two coaxially aligned infinitely flat half-filled disc coils as a function of the gap to diameter ratio according to (4) compared with an FEM simulation and a measurement.

III. AC Resistance

A. Ohmic Losses

There are two parts of the ohmic losses in the conductors of the coil, commonly referred to as skin- and proximity effect. For a round conductor, the power dissipated per unit length is

$$P'_\mathrm{r} = R'_{\mathrm{r,dc}}(F_\mathrm{r}\hat{I}_\mathrm{r}^2 + G_\mathrm{r}\hat{H}^2) \quad (5)$$

with its dc resistance per unit length $R'_{\mathrm{r,dc}}$, the current amplitude $\hat{I}_\mathrm{r}$ in the conductor, the external magnetic field amplitude $\hat{H}$ it is

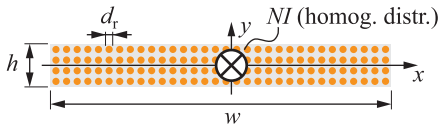

$$k_{cu} = \frac{N_r \frac{d_r^2 \pi}{4}}{hw}$$

Fig. 4. Infinitely long (z-direction) winding with a flat rectangular profile.

exposed to, and the frequency dependent skin- and proximity effect functions for round conductors F_r and G_r as provided in [9].

In a winding consisting of multiple round conductors, which may be part of a litz wire or simply the turns of one solid round wire, the magnetic field is generally not homogeneous. However, since the losses are proportional to the square of the magnetic field, the spatial RMS value of the magnetic field [9] within the winding volume $\mathscr{V}$

$$\hat{H}_{srms} = \sqrt{\frac{1}{V}\int_{\mathscr{V}} \hat{H}^2 \mathrm{dV}} \tag{6}$$

can be used to describe the total ohmic losses of the winding as

$$P_{ohm} = N_r l_w R'_{r,dc}(F_r \hat{I}_r^2 + G_r \hat{H}_{srms}^2) \tag{7}$$

with the total number of round conductors N_r contained in the winding, the mean winding length l_w, and the spatial RMS value of the magnetic field amplitude $\hat{H}_{srms}$. It is assumed that the round wires N_r, i.e., the strands of the winding are homogeneously distributed within the winding cross-section, therefore no internal proximity effect needs to be considered. This assumption is true in particular for rectangular profile litz wires but also a good approximation for tightly wound round profile litz wires.

The effective magnetic field length

$$l_h = \frac{N\hat{I}}{\hat{H}_{srms}} \tag{8}$$

is introduced to describe the proportionality between winding amp-turns amplitude $N\hat{I}$ and spatial RMS value of the magnetic field amplitude $\hat{H}_{srms}$. With (7) and (8), the ac resistance of the winding due to ohmic losses

$$R_{ohm} = 2R_{dc}\left(F_r + G_r\left(\frac{N_r}{l_h}\right)^2\right) \tag{9}$$

can be expressed as multiple of the winding dc resistance.

The tricky part is to calculate the effective magnetic field length l_h. An analytic approach is possible for a flat rectangular profile filled with round conductors as shown in Fig. 4. It is assumed that the number of conductors is high and that the profile is flat ($h \ll w$). Based on Ampère's law, the x-component of the magnetic field for $h \to 0$

$$H_x \simeq \frac{NI}{wh} y \tag{10}$$

is derived. Using the Biot–Savart law, the y-component

$$H_y \simeq \frac{NI}{2\pi w}\int_{-\frac{w}{2}}^{\frac{w}{2}} \frac{1}{x'-x}\mathrm{dx}' = \frac{NI}{2\pi w}\ln\left(\frac{\frac{w}{2}-x}{\frac{w}{2}+x}\right) \tag{11}$$

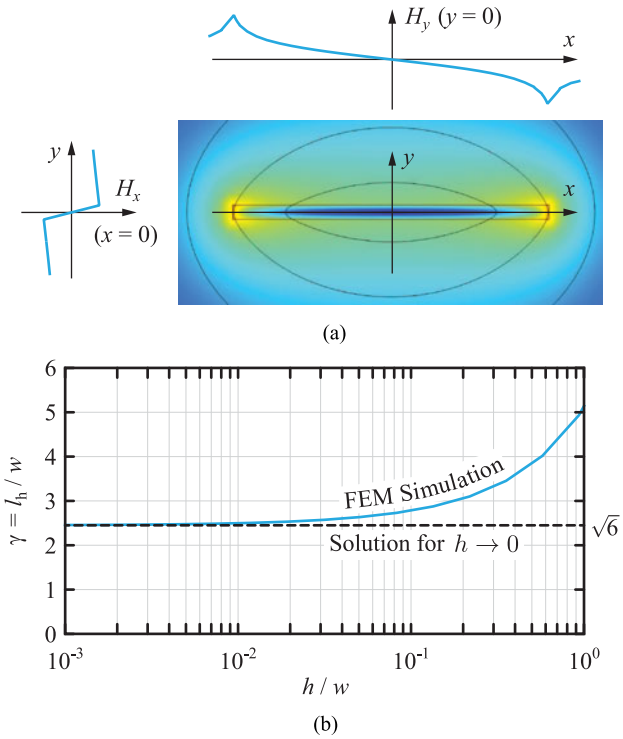

Fig. 5. (a) 2-D FEM simulation of the magnetic field and (b) effective magnetic field length [cf. (8)] per width of a flat rectangular winding.

follows and the magnetic field spatial RMS value of the flat rectangular winding profile

$$H_{srms} = \sqrt{\frac{1}{h}\int_{-\frac{h}{2}}^{\frac{h}{2}} H_x^2 \mathrm{dy} + \frac{1}{w}\int_{-\frac{w}{2}}^{\frac{w}{2}} H_y^2 \mathrm{dx}} = \frac{NI}{\sqrt{6}w} \tag{12}$$

is obtained. Since (12) is time independent, it is valid for instantaneous, amplitude, or RMS values of current I and spatial RMS magnetic field H. Therefore, the ratio of effective magnetic field length to width for the flat rectangular profile asymptotically equals as follows:

$$\gamma = \frac{l_h}{w} \simeq \sqrt{6} \tag{13}$$

for $h \to 0$. This result is verified using an FEM simulation shown in Fig. 5. As long as the winding is flat ($\frac{h}{w} < 0.1$), the solution for $h \to 0$ can be used with a good accuracy and the proximity losses are overestimated by less than 30%.

As shown in Fig. 6, the solution for the magnetic field of the flat rectangular profile can also be applied with a reasonable accuracy for one of the flat half-filled disc coils as defined in Fig. 2. For coils with $h < 0.05d$, the error in the proximity losses is within $\pm 22\%$.

In case of a pair of coils, the magnetic field of one coil also generates eddy currents in the other coil and vice versa. Assuming that the two coils are equal and that the coil currents are orthogonal, as they should be for maximum efficiency (25), this effect can be taken into account by using the numerically found equivalent ratio of the magnetic field length per winding width γ according to Fig. 7. However, this effect can be neglected if

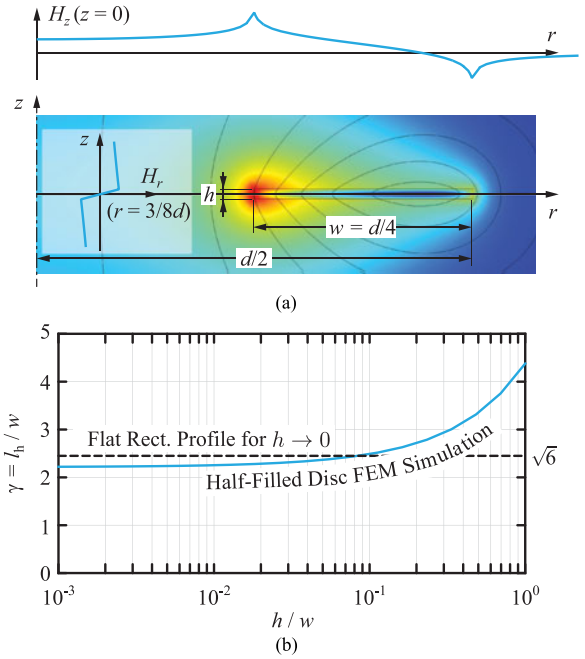

Fig. 6. (a) 2-D coaxial FEM simulation of the magnetic field and (b) effective magnetic field length per width of a flat half-filled disc winding.

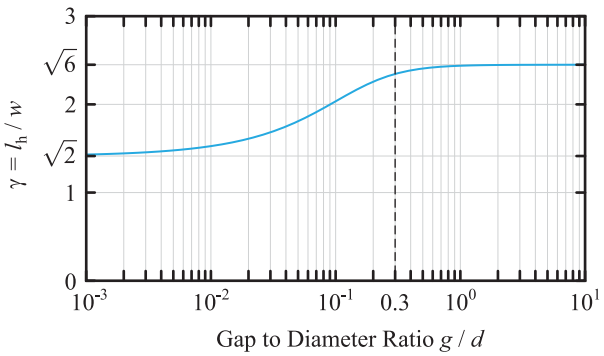

Fig. 7. Equivalent effective magnetic field length per winding width to include the proximity losses one coil of a pair of coils generates in the other identical coil.

the gap between the two flat-disc coils is larger than $0.3d$ (cf. limit indicated with dashed line in Fig. 7).

Each of the functions F_r and G_r in (9) can be replaced by an approximation for the low frequency (LF) range and by another approximation for the high frequency (HF) range as shown in the Appendix. For a winding, the LF range applies when the strand diameter d_r is less than $32^{\frac{1}{3}}\,\delta$, and the HF range applies for strand diameters larger than that. With the asymptotic approximations for F_r and G_r, the asymptotic approximations for the coil winding ac resistance in the LF range

$$R_{\mathrm{ohm,lf}} \simeq R_{\mathrm{dc}} \left(1 + \frac{k_{\mathrm{cu}}^2 h^2 d_r^2}{4\gamma^2 \delta^4}\right) \tag{14}$$

and the coil winding ac resistance in the HF range

$$R_{\mathrm{ohm,hf}} \simeq R_{\mathrm{dc}} \left(\frac{d_r}{4\delta} + \frac{8k_{\mathrm{cu}}^2 h^2}{\gamma^2 \delta d_r}\right) \tag{15}$$

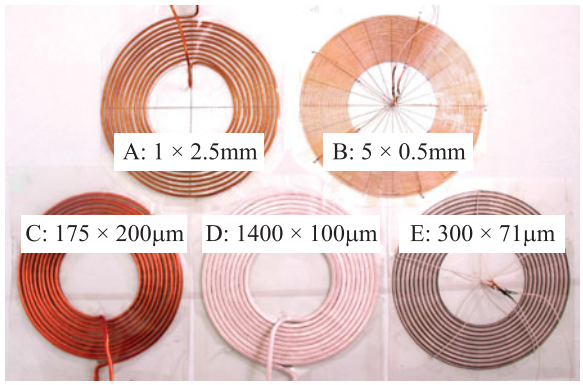

Fig. 8. Coil samples with $d = 20$ cm used for the verification of the ohmic resistance model.

are obtained, with the filling factor k_{cu} and the diameter of the round conductors d_r as defined in Fig. 4, the skin depth $\delta = \frac{1}{\sqrt{\pi \mu_0 \sigma f}}$ and the coil dc resistance is as follows:

$$R_{\mathrm{dc}} = N^2 \frac{3\pi}{k_{\mathrm{cu}} \sigma h}. \tag{16}$$

Since with increasing coil height h, the dc resistance decreases but the proximity losses increase [(14) and (15)], there is a loss in optimum coil height for the LF range

$$h_{\mathrm{opt,lf}} \simeq \frac{2\gamma\delta^2}{k_{\mathrm{cu}} d_r} \tag{17}$$

and also for the HF range

$$h_{\mathrm{opt,hf}} \simeq \frac{\gamma d_r}{4\sqrt{2} k_{\mathrm{cu}}}. \tag{18}$$

With the coil height set to the according optimum, the minimum ohmic resistances

$$R_{\mathrm{ohm,lf,min}} \simeq \frac{N^2 3\pi}{\sigma} \frac{d_r}{\gamma\delta^2} \tag{19}$$

and

$$R_{\mathrm{ohm,hf,min}} \simeq \frac{N^2 3\pi}{\sigma} \frac{2\sqrt{2}}{\gamma\delta} \tag{20}$$

can be obtained. It is observed that the minimum resistance in the LF range (19) equals $2R_{\mathrm{dc}}(h_{\mathrm{opt,lf}})$. Therefore, the optimum winding height for a given frequency is reached when the ac to dc resistance ratio at that frequency equals 2. It is further observed that the minimum resistance in the HF range (20) is independent of the wire diameter d_r. This result is confirmed by the ac resistance measurements obtained on coil sample A with a wire diameter of $d_r = 2.5$ mm and coil sample B with a wire diameter of $d_r = 0.5$ mm shown in Fig. 8. Both samples A and B use a single layer construction with the space between the turns set such that (18) is satisfied. In order to obtain the same number of turns of $N = 10$, five wires are symmetrically paralleled in sample B, while only a single wire is used for sample A. The measurements in Fig. 9 show that the ac resistances of the two coils in the HF range are indeed equal and that, since (18) is satisfied, the minimum ac resistance value for the HF range according to (20) is reached. Further measurements using litz

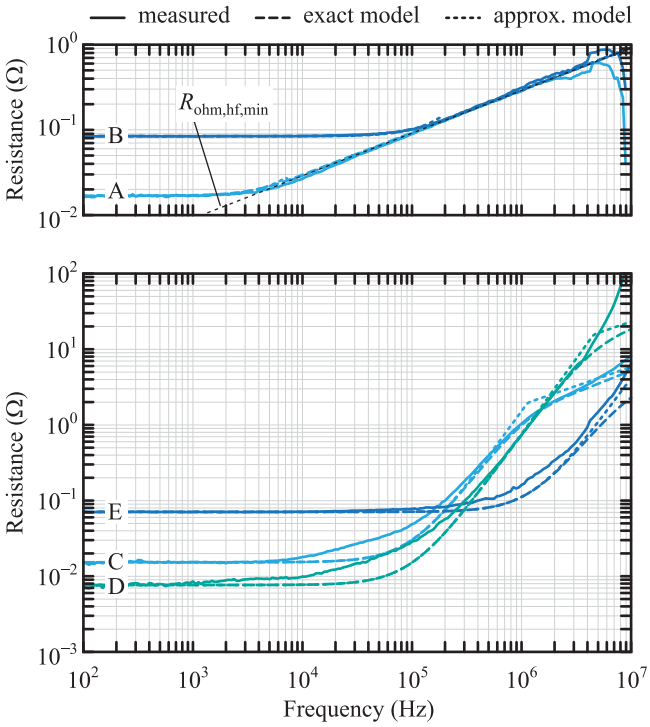

Fig. 9. Measured resistances of the coil samples in Fig. 8 compared to the exact expression for the ohmic resistance (9) and its approximations (14) and (15).

wire obtained from the coil samples C–E show a deviation from the predicted value of the model at the frequency where the proximity losses start to dominate. This can be explained by the nonideal twisting of a real litz wire [10], [11].

B. Radiated Losses

Apart from ohmic losses in the conductors of the coil, the radiated power also contributes to the losses [4]. One coil forms a magnetic dipole radiating [12]

$$P_{\mathrm{rad}} = \frac{\mu_0 \omega^4}{6\pi c_0^3} M^2 \tag{21}$$

with the RMS magnetic dipole moment

$$M = \frac{7\pi}{48} d^2 N I \tag{22}$$

of a half-filled disc coil. Each coil also forms an electric dipole; however, by keeping the voltage at the coil terminals low, using a low number of turns or a distributed compensation capacitor, this can be neglected. Therefore, the equivalent resistance for the radiated power $P_{\mathrm{rad}} = R_{\mathrm{rad}} I^2$ of one flat half-filled disc coil is

$$R_{\mathrm{rad}} = N^2 \frac{7^2 \pi^5}{3^3 2^5} \sqrt{\frac{\mu_0}{\varepsilon_0}} \left(\frac{df}{c_0}\right)^4. \tag{23}$$

IV. Efficiency Limit

The efficiency for power transfer from the primary to the secondary coil [cf. Fig. 1 and (1)] is

$$\eta_{12} = 1 - \frac{R_1 I_1^2 + R_2 I_2^2}{R_1 I_1^2 + \omega L_{\mathrm{m}} I_1 I_2 \sin(\varphi_{12})}. \tag{24}$$

For a given power transfer according to (1), there are three electrical degrees of freedom to maximize this efficiency: the phase shift between the primary and secondary current, the ratio between primary and secondary current amplitude, and the frequency.

A. Optimum Phase Shift

Independent of the values of currents, resistances, mutual inductance, and frequency, the efficiency (24) is always maximized for

$$\varphi_1 - \varphi_2|_{\mathrm{opt}} = \frac{\pi}{2}. \tag{25}$$

B. Optimum Current Ratio

From (24) with optimum phase shift, the optimum current ratio

$$\left.\frac{I_1}{I_2}\right|_{\mathrm{opt}} = \sqrt{\frac{R_2}{R_1}} \left(\frac{1}{kQ} + \sqrt{1 + \left(\frac{1}{kQ}\right)^2}\right) \simeq \sqrt{\frac{R_2}{R_1}} \tag{26}$$

is determined, which results in the maximum efficiency

$$\eta_{12,\mathrm{opt}} = \frac{1}{\left(\frac{1}{kQ} + \sqrt{1 + \left(\frac{1}{kQ}\right)^2}\right)^2} \simeq 1 - \frac{2}{kQ} \tag{27}$$

with the total quality factor of the coil pair

$$Q = \sqrt{Q_1 Q_2} = \sqrt{\frac{\omega L_1}{R_1} \frac{\omega L_2}{R_2}}. \tag{28}$$

For high values of kQ, the asymptotic approximations can be used.

C. Optimum Frequency

The coil pair efficiency (27) with optimum current ratio and optimum phase shift is maximized if the product kQ is maximized. While the coupling coefficient k does not depend on the frequency, the coil quality factor does. In the following, it is assumed that the quality factors of the two coils are equal, which is the case if their diameters d and strand diameters d_{r} are equal. Therefore, the optimum frequency is found at

$$Q_{\max} = \max_f \left(\frac{2\pi f L}{R_{\mathrm{ohm}}(f) + R_{\mathrm{rad}}(f)}\right). \tag{29}$$

The quality factor as function of the frequency of a flat disc coil with diameter $d = 20$ cm is shown in Fig. 10 for different strand diameters. The coil height is set to minimize the ohmic resistance according to (17) and (18) but it is limited to $h \leq 0.05$ d. Depending on the strand diameter, three different types of maxima of the coil quality factor can be identified, which can

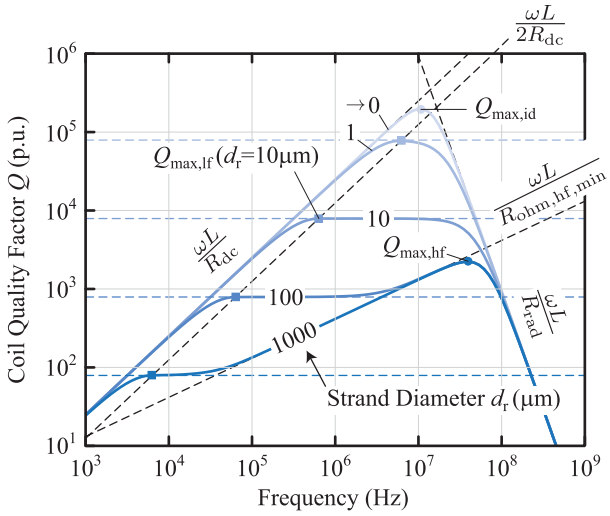

Fig. 10. Quality factor Q of a flat disc coil with diameter $d = 20$ cm as function of the frequency for different strand diameters. The coil height is set to the optimum value but limited to $h < 0.05$ d.

be expressed explicitly using the LF and HF approximations of the ohmic resistance.

1) Ideal Coil: If the strand diameter is infinitesimal small ($d_r \to 0$), the ohmic part of the coil resistance equals the dc resistance. However, the radiation resistance R_{rad} is proportional to f^4, while the reactance ωL is proportional to f. In this case, the maximum quality factor

$$Q_{max,id} \approx \frac{0.76}{\pi}\left(\frac{54}{49}\right)^{\frac{1}{4}}\left(k_{cu}\sigma d h_{max}\sqrt{\frac{\mu_0}{\varepsilon_0}}\right)^{\frac{3}{4}} \tag{30}$$

is reached at

$$f_{opt,id} = \frac{c_0}{\pi d}\left(\frac{2^5 3^3}{7^2 k_{cu}\sigma h_{max}\sqrt{\frac{\mu_0}{\varepsilon_0}}}\right)^{\frac{1}{4}} \tag{31}$$

with the coil height set to its maximum value h_{max}. This case marks the theoretical maximum of the quality factor, although in practice it is hardly relevant since it would require strands with a diameter of less than 1 µm which are twisted ideally.

2) LF Range: If the strand diameter is not infinitely small but still less than $\approx 3\delta$, the LF approximation applies for the ohmic resistance. In this case, with the coil height set to the optimum value according to (17), the ohmic resistance is proportional to the frequency (19). Since also the reactance is proportional to the frequency, the quality factor of the coil in the LF range is constant as long as the radiation resistance is negligible. This LF plateau of the quality factor is observed for a strand diameter $d_r = 10$ µm in the example of Fig. 10. At low frequencies, the optimum coil height would exceed the maximum coil height, set to $h_{max} = 0.05d$ in this example, and the plateau is therefore limited by $\frac{\omega L}{R_{dc}}$. At high frequencies, the rapidly increasing ($\propto f^4$) radiation resistance cuts off the plateau. The maximum of the LF plateau quality factor

$$Q_{max,lf} \approx \frac{2 \cdot 0.76 \cdot \gamma d}{3\pi d_r} \tag{32}$$

is reached at the lower frequency end of the plateau

$$f_{opt,lf} \approx \frac{2\gamma}{\pi\mu_0\sigma k_{cu} d_r h}. \tag{33}$$

If the coil height h is set to the maximum value h_{max}, the minimum operating frequency results, but also thinner coils with higher operating frequency achieve the same Q. In practice, the operating frequency will be determined by the semiconductors available and the coil height adjusted accordingly.

3) HF Range: If the strand diameter is larger than $\approx 3\delta$, the HF approximation for the ohmic resistance applies and the minimum ohmic resistance of the coil at optimum height is proportional to $\sqrt{f}$ (20). With the reactance proportional to f, the quality factor increases with $\sqrt{f}$ until the radiation resistance starts to dominate. In the example shown in Fig. 10, this is observed for a strand diameter $d_r = 100$ µm. At LF, the already discussed plateau is observed which is left at ≈ 4 MHz when the skin depth reaches $\approx \frac{d_r}{3}$. From that point on, the quality factor increases with $\sqrt{f}$ until the HF maximum of the quality factor

$$Q_{max,hf} \approx \frac{0.76}{\pi}\left(\frac{24}{343}\gamma^2\sigma d\sqrt{\frac{\mu_0}{\varepsilon_0}}\right)^{\frac{3}{7}} \tag{34}$$

is reached at

$$f_{opt,hf} \approx \frac{c_0}{\pi d}\left(\frac{2^{11}3^6}{7^4\sigma d\gamma^2\sqrt{\frac{\mu_0}{\varepsilon_0}}}\right)^{\frac{1}{7}}. \tag{35}$$

The HF optimum of the quality factor is independent of the strand diameter, as long as it is larger than $\approx 3\delta$. In order to reach this optimum, a simple round wire coil is sufficient. The frequency which is necessary to reach the HF optimum is relatively high, but decreases with increasing coil diameter.

Which one of the three optima of the quality factor applies depends on the strand diameter. Although only approximative, the following boundaries separate the three regions. If the strand diameter is less than

$$d_{r,id-lf} \approx d\gamma\left(\frac{2^3 7^2}{3^7}\right)^{\frac{1}{4}}\left(k_{cu}\sigma h\sqrt{\frac{\mu_0}{\varepsilon_0}}\right)^{-\frac{3}{4}} \tag{36}$$

the coil can be considered ideal and the optimum frequency for that case (31) applies. If the strand diameter is larger than $d_{r,id-lf}$ but less than

$$d_{r,lf-hf} \approx \left(\frac{7^9\gamma d^4}{2^2 3^{10}\left(\sqrt{\frac{\mu_0}{\varepsilon_0}}\sigma\right)^3}\right)^{\frac{1}{7}} \tag{37}$$

the maximum quality factor occurs at the LF optimum frequency (33). And if the strand diameter is larger than $d_{r,lf-hf}$, the HF optimum (35) applies.

The maximum quality factor and the optimum operating frequency for a flat disc coil with $h < 0.05d$ as function of the coil diameter are shown in Fig. 11 for different strand diameters. For a strand diameter of 71 µm, the border between HF and LF optimum (37) is observed at a coil diameter of ≈ 65 µm.

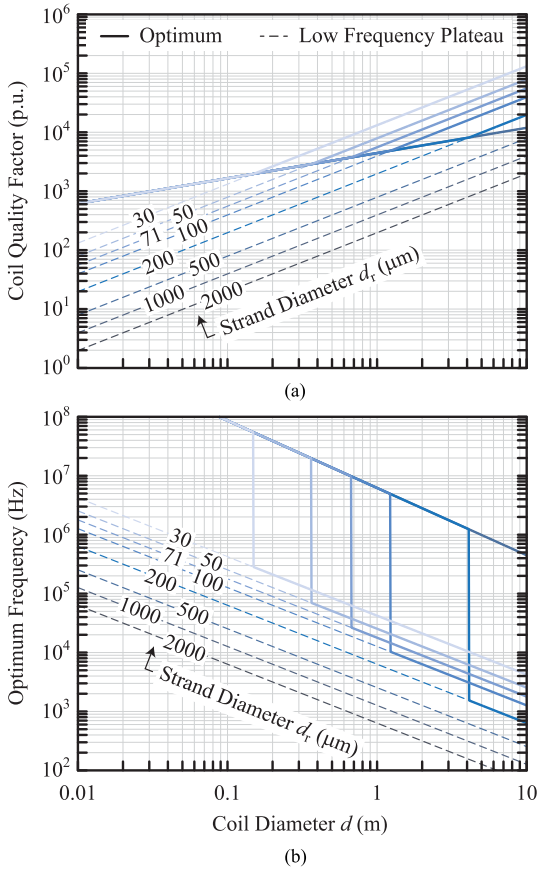

Fig. 11. (a) Maximum coil quality factor (solid lines) at optimum height and optimum frequency and (b) the required operating frequency depending on coil diameter d and strand diameter d_r of a flat (h <0.05 d) disc coil. (a) Dashed lines indicate the suboptimal quality factor and (b) corresponding frequency at the LF plateau.

If the coil diameter is larger than that, the LF plateau marks the optimum. If the maximum coil height of $0.05d$ is used, the optimum operating frequency of a 65 cm coil is only 30 kHz.

For coils with lower diameters than 65 cm, the quality factor at the LF plateau is lower than at the HF optimum (cf. Fig. 10 with $d_\mathrm{r} = 100$ µm). The optimum operating frequency is defined by (35), resulting in values higher than 10 MHz for this example, which is typically unacceptable due to the inverter switching losses. Also coil resonance becomes an issue in the HF range, requiring measures such as a coil integrated compensation capacitance.

In practice, smaller coils should therefore be equipped with lower strand diameters, which increases the quality factor at the LF plateau. Also if the strand diameter is not reduced, it likely makes sense to operate the coil at a suboptimal LF plateau instead of increasing the switching frequency by more than two orders of magnitude in order to reach the HF optimum.

D. Coil Pair Efficiency Limit With a 71 µm Strand Diameter

Depending on the coil diameter d and gap g, the coil pair efficiency is shown for the 71 µm strand diameter in Fig. 12 for the case that the coil is operated at the global optimum of the quality factor (solid line) and for the case it is operated

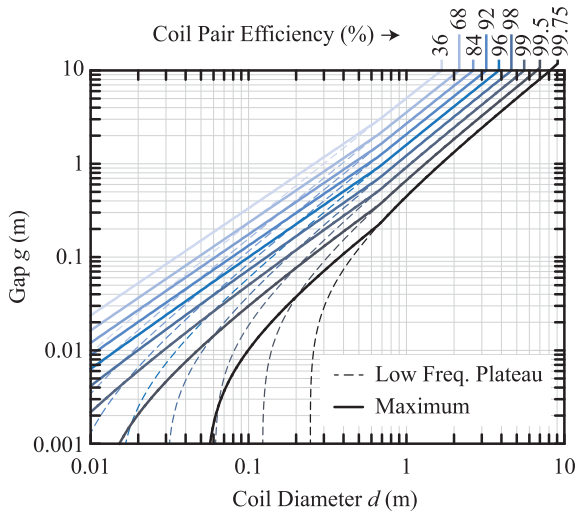

Fig. 12. IPT efficiency of a pair of identical flat half-filled disc coils with 71 µm strand diameter as function of coil diameter d and gap g at the global frequency optimum (solid line) and at the LF plateau of the quality factor (dashed line).

at the LF plateau (dashed line). For coil diameters larger than 65 cm, the LF plateau constitutes the global optimum. With lower coil diameters, the HF optimum of the quality factor applies. Operating the coil pair at the LF plateau instead results in lower efficiency but at the same time in an orders of magnitude lower operating frequency. For example, a coil diameter of 20 cm at a gap of 30 cm, the efficiency at the (HF) optimum is 92% with 40 MHz operating frequency, whereas the efficiency at the LF plateau is 84% at 90 kHz.

E. Thermal Power Limit With the 71 µm Strand Diameter

Often the required coil pair efficiency is not specified, instead the coil is dimensioned for a temperature limit that must not be exceeded at the maximum output power and maximum gap. Assuming the typical case of natural convection and radiation cooling, a coil temperature limit of 100 °C and an ambient temperature of 40 °C, the maximum surface loss density must be limited to <900 W/m^2 [13].

For a pair of coils with 71 µm litz wire and only one of the two surfaces of each coil available for cooling, the thermal output power limit is shown in Fig. 13.

F. Rule of Thumb for the LF Plateau

The operating frequency at the LF plateau depends on the coil height (17) and can therefore be adjusted to fit the inverter capabilities. Therefore, the LF plateau is exploited in a wide range of applications. Two rule of thumb expressions for the LF plateau shall summarize the analysis. Combining (32), and the approximations of (27) and (4) results in the approximative efficiency of a pair of flat disc coils at the LF plateau of

$$\eta \approx 1 - \frac{5d_\mathrm{r}}{d}\left(1 + 3.2\left(\frac{g}{d}\right)^2\right)\left(1 + 7\frac{g}{d}\right). \qquad (38)$$

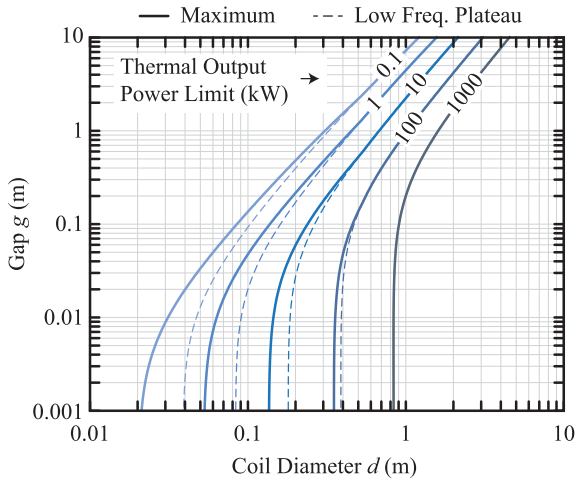

Fig. 13. Thermal output power limit of a pair of identical flat half-filled disc coils with 71 µm strand diameter as function of coil diameter d and gap g at the global frequency optimum (solid line) and at the LF plateau of the quality factor (dashed line) assuming a maximum surface loss density of 900 W/m^2.

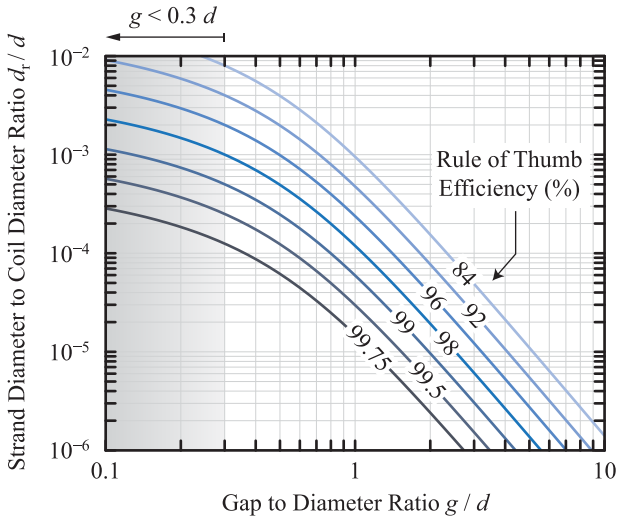

Fig. 14. Efficiency at the LF plateau according to the rule of thumb (38) as a function of the gap to coil diameter ratio and the strand diameter to coil diameter ratio.

This approximation is valid if the efficiency is higher than 90% and the coils are separated by $g > 0.3d$. The efficiency limit according to (38) is shown in Fig. 14.

The second rule of thumb expression sets the coil height according to the optimum value for the LF plateau (17) as

$$h \approx \frac{1.5}{\mu_0 \sigma k_{\mathrm{cu}} d_{\mathrm{r}} f} \tag{39}$$

depending on the selected frequency f and strand diameter d_{r}.

The approximate efficiency expression (38) shows that the only way to increase the efficiency for a given coil diameter d and gap g is to reduce the strand diameter d_{r}. However, reducing the strand diameter comes at the price of higher switching frequency, since according to (39), the optimum operating frequency of an IPT coil pair at the LF plateau is inversely proportional to the product of the strand diameter and coil height. This is similar to the optimum operating frequency of transformers (cf. [9, (21)]), which is inversely proportional to the product of the winding width and strand diameter.

V. Conclusion

The efficiency limit for IPT between two flat disc coils has been derived, based on analytic approximations for the frequency dependency of the coil resistance and the coupling coefficient. Both approximations are verified experimentally.

Based on the conditions for maximum transfer efficiency—orthogonal coil currents, equal loss sharing between the coils, and maximum quality factor—it is shown that the analytic approximations can be used to derive two different optima for the operating frequency that maximize the efficiency.

At first, the LF optimum is applied, if the coil is made of a litz wire thin enough (37). In this case, the optimum frequency is reached when the coil's ac to dc resistance ratio is 2. This frequency is inversely proportional to the coil height and can thus be selected to fit the inverter capabilities. At the LF optimum, the efficiency only depends on the coil diameter, the strand diameter, and the gap between the coils.

If the strand diameter exceeds a certain value, the optimum frequency occurs at the HF optimum, which is typically in the range of tens of megahertz [cf. (37)]. This second kind of optimum is not affected by the strand diameter of the coil and therefore provides more flexibility for the construction of the coil, although the required switching frequency is only determined by the coil diameter and cannot be varied by varying the thickness of the coil as it is the case in the LF optimum.

In practice, the LF optimum is often preferred due to its lower frequency, which is typically in the tens to hundreds of Kilohertz range. For the case of two flat-disc coils, a rule of thumb is presented to calculate the LF coil pair efficiency based on strand diameter, coil diameter, and gap between the coils.

Appendix

The exact expressions of F_{r} and G_{r} are relatively complex and involve Kelvin functions. For conductor diameters much smaller or larger than $\approx 3\delta$, the following asymptotic approximations can be used:

$$F_{\mathrm{r}} \simeq \begin{cases} \dfrac{1}{2}, & \text{if } d_{\mathrm{r}} < 4\delta \\ \dfrac{d_{\mathrm{r}}}{8\delta}, & \text{if } d_{\mathrm{r}} \geq 4\delta \end{cases} \tag{40}$$

$$G_{\mathrm{r}} \simeq \begin{cases} \dfrac{\pi^2 d_{\mathrm{r}}^6}{128\delta^4}, & \text{if } d_{\mathrm{r}} < 32^{\frac{1}{3}}\delta \\ \dfrac{\pi^2 d_{\mathrm{r}}^3}{4\delta}, & \text{if } d_{\mathrm{r}} \geq 32^{\frac{1}{3}}\delta \end{cases}. \tag{41}$$

References

[1] R. Bosshard, T. Guillod, and J. W. Kolar, "Electromagnetic field patterns and energy flux of efficiency optimal inductive power transfer systems," *Electr. Eng.*, vol. 99, no. 3, pp. 969–977, 2016.

[2] E. Waffenschmidt and T. Staring, "Limitation of inductive power transfer for consumer applications," in *Proc. 13th Eur. Conf. Power Electron. Appl.*, 2009, pp. 1–10.

[3] J. C. Schuder, "Powering an artificial heart: Birth of the inductively coupled-radio frequency system in 1960," *Artif. Organs*, vol. 26, no. 11, pp. 909–915, 2002.
[4] A. Kurs, A. Karalis, R. Moffatt, J. D. Joannopoulos, P. Fisher, and M. Soljačić, "Wireless power transfer via strongly coupled magnetic resonances," *Science*, vol. 317, no. 5834, pp. 83–86, 2007.
[5] J. Choi, D. Tsukiyama, Y. Tsuruda, and J. Rivas, "13.56 MHz 1.3 kw resonant converter with GAN FET for wireless power transfer," in *Proc. IEEE Wireless Power Transfer Conf.*, 2015, pp. 1–4.
[6] R. Bosshard and J. W. Kolar, "Multi-objective optimization of 50 kw/85 khz IPT system for public transport," *IEEE J. Emerg. Sel. Topics Power Electron.*, vol. 4, no. 4, pp. 1370–1382, Dec. 2016.
[7] R. Bosshard, J. W. Kolar, J. Mühlethaler, I. Stevanović, B. Wunsch, and F. Canales, "Modeling and η-α-pareto optimization of inductive power transfer coils for electric vehicles," *IEEE J. Emerg. Sel. Topics Power Electron.*, vol. 3, no. 1, pp. 50–64, Mar. 2015.
[8] S. Babic, S. Salon, and C. Akyel, "The mutual inductance of two thin coaxial disk coils in air," *IEEE Trans. Magn.*, vol. 40, no. 2, pp. 822–825, Mar. 2004.
[9] M. Leibl, G. Ortiz, and J. W. Kolar, "Design and experimental analysis of a medium-frequency transformer for solid-state transformer applications," *IEEE J. Emerg. Sel. Topics Power Electron.*, vol. 5, no. 1, pp. 110–123, Mar. 2017.
[10] H. Rossmanith, M. Doebroenti, M. Albach, and D. Exner, "Measurement and characterization of high frequency losses in nonideal litz wires," *IEEE Trans. Power Electron.*, vol. 26, no. 11, pp. 3386–3394, Nov. 2011.
[11] T. Guillod, J. Huber, F. Krismer, and J. W. Kolar, "Litz wire losses: Effects of twisting imperfections," in *Proc. 18th IEEE Workshop Control Model. Power Electron.*, Jul. 2017, pp. 1–8.
[12] S. Silver, *Microwave Antenna Theory and Design*, vol. 19. Stevenage, U.K.: IET, 2008.
[13] Y. Shabany, *Heat Transfer: Thermal Management of Electronics*. Boca Raton, FL, USA: CRC Press, 2009.

Michael Leibl (M'12) received the B.Sc. degree from the Vienna University of Technology, Vienna, Austria, in 2010, and the M.Sc. degree from the Swiss Federal Institute of Technology, Zurich, Switzerland, in 2012, both in electrical engineering.

Until 2017, he was with the Power Electronic Systems Laboratory working on his Ph.D. thesis on three-phase rectifiers and high-voltage supplies for X-ray systems, covering his main research interests which include optimized design of inductive components, in particular modeling high-frequency winding loss, high-power three-phase PFC rectifiers, and isolated dc–dc converters. He is currently a Predevelopment Engineer with Brusa Elektronik AG, Sennwald, Switzerland.

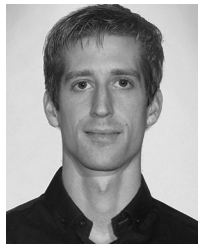

Oliver Knecht (S'14) received the M.Sc. degree in electrical engineering from the Swiss Federal Institute of Technology, Zurich, Switzerland, in 2013.

Until 2017, he was with the Power Electronic Systems Laboratory working on his Ph.D. thesis with the title "Transcutaneous energy and information transfer for left ventricular assist devices." During his studies, he focused on power electronics, control systems, and microwave electronics. His research interests include the analysis, design, and control of inductive power transfer systems for medical applications. He is currently working as an R&D Engineer at Onefive GmbH, Regensdorf, Switzerland (part of NKT Photonics A/S).

Johann W. Kolar (F'10) received the Ph.D. degree (summa cum laude) in electrical engineering from the Vienna University of Technology, Vienna, Austria.

He is currently a Full Professor and the Head of the Power Electronic Systems Laboratory, Swiss Federal Institute of Technology, Zurich, Switzerland. He has proposed numerous novel PWM converter topologies, and modulation and control concepts and has supervised more than 60 Ph.D. students. He has published more than 750 scientific papers in international journals and conference proceedings, 3 book chapters, and has filed more than 140 patents. He has initiated and/or is the founder of four ETH Spin-off companies. His current research interests include ultracompact and ultraefficient SiC and GaN converter systems, wireless power transfer, solid-state transformers, power supplies on chip, as well as ultrahigh speed and ultralight weight drives, bearingless motors, and energy harvesting.

Dr. Kolar has presented more than 20 educational seminars at leading international conferences, has served as IEEE PELS Distinguished Lecturer from 2012 through 2016, and has received 25 IEEE Transactions and Conference Prize Paper Awards, the 2014 IEEE Power Electronics Society R. David Middlebrook Achievement Award, the 2014 SEMIKRON Innovation Award, the 2016 IEEE William E. Newell Power Electronics Award, the 2016 IEEE PEMC Council Award, and the ETH Zurich Golden Owl Award for excellence in teaching.